APPLIED GEOPHYSICS, Vol.6, No.2 (June 2009), P. 113 - 121, 5 Figures.
DOI:10.1007/s11770-009-0012-3

The implementation of an improved NPML absorbing boundary condition in elastic wave modeling*

Qin Zhen[1, 2], Lu Minghui[1], Zheng Xiaodong[1], Yao Yao[2], Zhang Cai[1], and Song Jianyong[3]

Abstract: In elastic wave forward modeling, absorbing boundary conditions (ABC) are used to mitigate undesired reflections from the model truncation boundaries. The perfectly matched layer (PML) has proved to be the best available ABC. However, the traditional splitting PML (SPML) ABC has some serious disadvantages: for example, global SPML ABCs require much more computing memory, although the implementation is easy. The implementation of local SPML ABCs also has some difficulties, since edges and corners must be considered. The traditional non-splitting perfectly matched layer (NPML) ABC has complex computation because of the convolution. In this paper, based on non-splitting perfectly matched layer (NPML) ABCs combined with the complex frequency-shifted stretching function (CFS), we introduce a novel numerical implementation method for PML absorbing boundary conditions with simple calculation equations, small memory requirement, and easy programming.
Keywords: PML, absorbing boundary condition, non-splitting, forward modeling

Introduction

In finite-difference time-domain modeling, the perfectly matched layer (PML) absorbing boundary condition (ABC) has proven to be the most robust and efficient for Maxwell's electromagnetic and elastic waves (Berenger, 1994). The elastic wave equation for PML media has become the conventional wave equation. In this media, the wave phase does not change but the amplitude changes due to exponential decay during wave propagation. For the perfectly matched layer having the same elastic parameters and different attenuation coefficients, the impedances are perfectly matched. Theoretically, there is no boundary reflection and the reflections are mainly caused by numerical dispersion. Chew and Weedon (1994) formulated the PML ABC by applying a complex stretch coordinate. Rappapport (1995) proved that the PML is equivalent to anisotropic media in the absorption area. Many examples (Chew and Weedon, 1994; Chen et al., 1997) demonstrated that the absorption of the PML absorbing boundary condition is much better than exponential attenuation ABCs (Marfurt, 1984; Shin, 1995), Mur ABCs (Liao et al., 1984), and Higdon ABCs (Higdon, 1991). Chen et al. (1997) and Wang and Oristaglio (2000) successfully applied PML ABCs to solve the electromagnetic wave equation. In recent years, the PML was widely applied in acoustic and elastic wave finite-difference forward modeling (Rappapport, 1995; Chew and Liu, 1996; Hastings et al., 1996; Komatitsch and Tromp, 1999; Collino and Tsogka, 2001; Festa and Nielsen, 2003; Basu and Chopra, 2004; Cohen and Fauqueux, 2005; Festa and Vilotte, 2005; Appelö and Kreiss, 2006; Ma and Liu, 2006). Teixeira

Manuscript received by the Editor December 2008, revised manuscript received March 25, 2009.
*This research was sponsored by the Chinese National Development and Reform Commission (No. [2005]2372) and the Innovative Technological Research Foundation of PetroChina Company Limited (No. 060511-1-3).
1.Research Institute of Petroleum Exploration & Development, Beijing 100083, China.
2. Institute of Geophysics & Geomatics , China University of Geosciences, Wuhan 430074, China.
3. Faculty of Resource & Information, China University of Petroleum, Beijing 102249, China.

and Chew (1999) extended PML ABCs to cylindrical and spherical coordinates. Song et al. (2005) applied NPML ABCs to elastic wave numerical modeling in poroelastic media.

At present, the PML realization has a variety of forms, of which the main ones are splitting and non-splitting PMLs. The two different implementation methods have the same absorption effect for artificial boundary reflections. The SPML is implemented by splitting the original field components and its equation is very simple. The SPML also can be divided into global and local SPML. For the global SPML, we can use the same PML wave equations in both the modeling and attenuation areas. The algorithm is easy to realize, although the introduction of auxiliary variables requires large memory However, it is only applicable to 2-D forward modeling and not to the 3-D case. For the local PML, in the modeling area we use conventional wave equations and in the attenuation area we use PML wave equations, thus saving a lot of memory However, it is difficult to program due to the many different boundaries and corners. The NPML has an advantage because it does not need to split the field components in the PML region. The convolution PML (CPML) needs to do many convolution operations in the time domain. In the past, the NPML algorithm was considered to be complex, with a large amount of computations, and not superior to the local SPML. So, until recently, the SPML was used in most wavefield forward modeling methods.

However, conventional PML ABCs cause large errors at boundary conditions near the wave source due to rapidly changing incidence angles and to using only one attenuation parameter. In addition, it doesn't absorb reflections from low-frequency boundaries as well as evanescent waves very well. Kuzuoglu and Mittra (1996) presented a complex frequency shifted (CFS) PML ABC to absorb evanescent waves and long time-varying signals by enlarging the real axis of the conventional complex stretching coordinate system and simply shifting the zero position of the virtual axis into the negative imaginary half. The PML ABC equations also can be applied to electromagnetic waves propagating in dispersive, lossy, inhomogeneous, anisotropic, and nonlinear media. Drossaert and Giannopoulos (2007) made a realization of the CFS in CPML by recursive integration. They used a recursive convolution operation to greatly reduce the time and memory. Compared with conventional stretch functions, the CFS stretch function has much more flexibility for modeling attenuation and absorption in PML media.

In this paper, we introduce a novel implementation of the CFS-PML. The NPML calculation in the time domain is decomposed into normal and attenuation terms using auxiliary variables, thus avoiding convolution operators. The implementation of the new method is described *i*n detail and the parameters are discussed. Finally, numerical tests validate the effectiveness of the new method.

Theory

Wave equations for PML media

In the complex stretch coordinates, the two-dimensional, elastic, first-order, stress-velocity difference wave equations are expressed as (Tsili and Tang, 2003; Drossaert and Giannopoulos, 2007):

$$\begin{cases} i\omega\rho\tilde{V}_x = \dfrac{\partial\tilde{T}_{xx}}{\partial\tilde{x}} + \dfrac{\partial\tilde{T}_{xz}}{\partial\tilde{z}} \\ i\omega\rho\tilde{V}_z = \dfrac{\partial\tilde{T}_{xz}}{\partial\tilde{x}} + \dfrac{\partial\tilde{T}_{zz}}{\partial\tilde{z}} \\ i\omega\tilde{T}_{xx} = (\lambda+2\mu)\dfrac{\partial\tilde{V}_x}{\partial\tilde{x}} + \lambda\dfrac{\partial\tilde{V}_z}{\partial\tilde{z}}, \\ i\omega\tilde{T}_{zz} = \lambda\dfrac{\partial\tilde{V}_x}{\partial\tilde{x}} + (\lambda+2\mu)\dfrac{\partial\tilde{V}_z}{\partial\tilde{z}} \\ i\omega\tilde{T}_{xz} = \mu\dfrac{\partial\tilde{V}_z}{\partial\tilde{x}} + \mu\dfrac{\partial\tilde{V}_x}{\partial\tilde{z}} \end{cases} \tag{1}$$

where $\lambda = \rho(\upsilon_p^2 - 2\upsilon_s^2), \mu = \rho\upsilon_s^2$, ρ is the density, υ_p is the primary wave velocity, and υ_s is the shear wave velocity. V_x *and* V_z are the horizontal and vertical particle velocity vectors; T_{xx}, T_{zz}, T_{xz} are the horizontal normal stress, vertical normal stress, and shear stress, respectively.

The frequency stretch coordinate (Tsili and Tang, 2003) is defined as

$$\tilde{p}(p) = \int_0^p \tilde{s}_p(p')dp', (p = x, y, z). \tag{2}$$

The stretch function (Tsili and Tang, 2003; Drossaert and Giannopoulos, 2007) is defined as

$$\tilde{s}_p = 1 + \frac{\sigma_p}{i\omega}, (p = x, y, z). \tag{3}$$

Differentiating equation (2), we have

$$\frac{\partial}{\partial\tilde{p}} = \frac{1}{\tilde{s}_p}\frac{\partial}{\partial p}, (p = x, y, z). \tag{4}$$

Substituting equations (3) and (4) into equation (1), the traditional PML equations can be derived in the Cartesian coordinate system.

Complex frequency stretch function

The modified complex frequency stretch function

(CFS) is defined as (Kuzuoglu and Mittra, 1996):

$$\tilde{s}_p(\omega)=\kappa_p+\frac{\sigma_p}{\alpha_p+i\omega},\ (p=x,y,z), \tag{5}$$

where κ and α are two additional attenuation parameters introduced into the stretch function. The parameter κ mainly affects the absorption of evanescent waves. The α parameter has an impact on the absorption of the low frequency component. Compared to the stretch function of equation (3), equation (5) magnifies the real axis of the coordinate system by κ and eliminates the low-frequency singularity by an α frequency shift of the virtual axis. Converting back into the time domain for both sides of equation (5), we get

$$\frac{1}{s_p(t)}=\frac{\delta(t)}{\kappa_p}-\frac{\sigma_p}{\kappa_p^2}e^{-(\frac{\sigma_p}{\kappa_p}+\alpha_p)t}=\frac{\delta(t)}{\kappa_p}+\xi_p(t),(p=x,y,z), \tag{6}$$

where

$$\xi_p(t)=\frac{\sigma_p}{\kappa_p^2}e^{-(\frac{\sigma_p}{\kappa_p}+\alpha_p)t}.$$

SPML absorbing boundary condition

The intention of SPML is to split the particle velocity and stress components in the coordinate direction. Taking the $\tilde{T}_{zz}$ component in the third equation of equation (1) as an example, we get

$$i\omega\tilde{T}_{xxx}=(\lambda+2\mu)\frac{1}{s_x}\frac{\partial\tilde{V}_x}{\partial x},i\omega\tilde{T}_{xxz}=\lambda\frac{1}{s_z}\frac{\partial\tilde{V}_z}{\partial z}, \tag{7}$$

where $\tilde{T}_{xx}=\tilde{T}_{xxx}+\tilde{T}_{xxz}$. s_x and s_z are defined by equation (3). The SPML wave equation is equivalent to the traditional equation when the absorption factor is zero.

NPML absorbing boundary condition

Substituting equation (6) into the third equation of equation (1), we get the equation in the time domain, i.e., the traditional expression of NPML equations:

$$\begin{aligned}\frac{\partial T_{xx}}{\partial t}&=(\lambda+2\mu)\frac{1}{\kappa_x}\frac{\partial V_x}{\partial x}+\lambda\frac{1}{\kappa_z}\frac{\partial V_z}{\partial z}\\&+(\lambda+2\mu)\xi_x(t)\otimes\frac{\partial V_x}{\partial x}+\lambda\xi_z(t)\otimes\frac{\partial V_z}{\partial z}.\end{aligned} \tag{8}$$

where $\otimes$ denotes convolution.

The CFS-PML implementation

To easily implement the CFS-PML ABC in the time domain, we present a new method based on the NSPML wave equation. First, the reciprocal of the CFS function in equation (5) is decomposed:

$$\frac{1}{\tilde{s}_p}=\frac{1}{\kappa_p}-\frac{\sigma_p}{\kappa_p^2[i\omega+(\alpha_p+\sigma_p/\kappa_p)]},(p=x,y,z). \tag{9}$$

Then we substitute equation (9) into the third equation of Equation (1)

$$\begin{aligned}i\omega\tilde{T}_{xx}&=(\lambda+2\mu)(\frac{1}{\kappa_x}\frac{\partial\tilde{V}_x}{\partial x}-\frac{\sigma_x}{\kappa_x^2[i\omega+(\alpha_x+\sigma_x/\kappa_x)]}\frac{\partial\tilde{V}_x}{\partial x})\\&+\lambda(\frac{1}{\kappa_z}\frac{\partial\tilde{V}_z}{\partial z}-\frac{\sigma_z}{\kappa_z^2[i\omega+(\alpha_z+\sigma_z/\kappa_z)]}\frac{\partial\tilde{V}_z}{\partial z})\end{aligned} \tag{10}$$

If equation (10) is transformed into the time domain directly, we will attain equation (8). However, this equation involves a convolution operation, resulting in additional computations and memory storage. To avoid this, some auxiliary variables are introduced in the frequency domain, resulting in equation (11):

$$\begin{cases}\tilde{\Psi}_{xx}=\dfrac{\sigma_x}{\kappa_x^2[i\omega+(\alpha_x+\sigma_x/\kappa_x)]}\dfrac{\partial\tilde{V}_x}{\partial x}\\ \tilde{\Psi}_{zz}=\dfrac{\sigma_z}{\kappa_z^2[i\omega+(\alpha_z+\sigma_z/\kappa_z)]}\dfrac{\partial\tilde{V}_z}{\partial z}\end{cases}. \tag{11}$$

Rearranging equation (11), we get

$$\begin{cases}i\omega\tilde{\Psi}_{xx}+(\alpha_x+\dfrac{\sigma_x}{\kappa_x})\tilde{\Psi}_{xx}=\dfrac{\sigma_x}{\kappa_x^2}\dfrac{\partial\tilde{V}_x}{\partial x}\\ i\omega\tilde{\Psi}_{zz}+(\alpha_z+\dfrac{\sigma_z}{\kappa_z})\tilde{\Psi}_{zz}=\dfrac{\sigma_z}{\kappa_z^2}\dfrac{\partial\tilde{V}_z}{\partial z}\end{cases}. \tag{12}$$

Comparing equations (11) and (12), if equation (11) is transformed into the time domain, the right-hand term is a convolution operation. If equation (12) is transformed into the time domain, the first left-hand term is also a convolution operator and is the time first-order partial derivative operator, whose calculation is easy.

Meanwhile, after introducing auxiliary variables, equation (10) becomes

$$i\omega\tilde{T}_{xx}=(\lambda+2\mu)\frac{1}{\kappa_x}\frac{\partial\tilde{V}_x}{\partial x}+\lambda\frac{1}{\kappa_z}\frac{\partial\tilde{V}_z}{\partial z}-(\lambda+2\mu)\Psi_{xx}-\lambda\Psi_{zz}. \tag{13}$$

To avoid effects from the CFS-PML attenuation parameter κ during implementation of conventional wave equation, we rewrite equation (13) as:

$$\begin{aligned}i\omega\tilde{T}_{xx}=&\left\{(\lambda+2\mu)\frac{\partial\tilde{V}_x}{\partial x}+\lambda\frac{\partial\tilde{V}_z}{\partial z}\right\}\\&-\left\{\begin{matrix}(\lambda+2\mu)[\Psi_{xx}+(1-\dfrac{1}{\kappa_x})\dfrac{\partial\tilde{V}_x}{\partial x}]\\+\lambda[\Psi_{zz}+(1-\dfrac{1}{\kappa_z})\dfrac{\partial\tilde{V}_z}{\partial z}]\end{matrix}\right\},\end{aligned} \tag{14}$$

Assisted by the introduction of auxiliary variables, the PML wave equation in the frequency domain can be divided into two parts: normal terms (the first term of the right side) and attenuated terms (the second term). If the

attenuated term is zero, the CFS-PML wave equations reduce to the normal wave equation because it is the sum of the relationship between them, Thus, equation (14) can be consider as an expansion of the elastic wave equations. Below is the complete set of 2D CFS-PML wave equations:

$$\begin{cases} \dfrac{\partial \Omega_{xx}}{\partial t}+(\alpha_x+\dfrac{\sigma_x}{\kappa_x})\Omega_{xx}=\dfrac{\sigma_x}{\kappa_x^2}\dfrac{\partial T_{xx}}{\partial x} \\ \dfrac{\partial \Omega_{xz}}{\partial t}+(\alpha_z+\dfrac{\sigma_z}{\kappa_z})\Omega_{xz}=\dfrac{\sigma_z}{\kappa_z^2}\dfrac{\partial T_{xz}}{\partial z} \\ \dfrac{\partial \Omega_{zx}}{\partial t}+(\alpha_x+\dfrac{\sigma_x}{\kappa_x})\Omega_{zx}=\dfrac{\sigma_x}{\kappa_x^2}\dfrac{\partial T_{xz}}{\partial x} \\ \dfrac{\partial \Omega_{zz}}{\partial t}+(\alpha_z+\dfrac{\sigma_z}{\kappa_z})\Omega_{zz}=\dfrac{\sigma_z}{\kappa_z^2}\dfrac{\partial T_{zz}}{\partial z} \\ \dfrac{\partial \Psi_{xx}}{\partial t}+(\alpha_x+\dfrac{\sigma_x}{\kappa_x})\Psi_{xx}=\dfrac{\sigma_x}{\kappa_x^2}\dfrac{\partial V_x}{\partial z} \\ \dfrac{\partial \Psi_{zz}}{\partial t}+(\alpha_z+\dfrac{\sigma_z}{\kappa_z})\Psi_{zz}=\dfrac{\sigma_z}{\kappa_z^2}\dfrac{\partial V_z}{\partial z} \\ \dfrac{\partial \Psi_{zx}}{\partial t}+(\alpha_x+\dfrac{\sigma_x}{\kappa_x})\Psi_{zx}=\dfrac{\sigma_x}{\kappa_x^2}\dfrac{\partial V_z}{\partial x} \\ \dfrac{\partial \Psi_{xz}}{\partial t}+(\alpha_z+\dfrac{\sigma_z}{\kappa_z})\Psi_{xz}=\dfrac{\sigma_z}{\kappa_z^2}\dfrac{\partial V_x}{\partial z} \end{cases}, \tag{15}$$

where $\Omega_{xx}, \Omega_{xz}, \Omega_{zx}, \Omega_{zz}$ and $\psi_{xx}, \psi_{xz}, \psi_{zx}, \psi_{zz}$ are the introduced auxiliary variables. By transforming equation (12) into the time domain and comparing other field components, we get the corresponding auxiliary control equations,

$$\frac{\partial \Omega_{xx}}{\partial t}+(\alpha_x+\frac{\sigma_x}{\kappa_x})\Omega_{xx}=\frac{\sigma_x}{\kappa_x^2}\frac{\partial T_{xx}}{\partial x} \tag{16a}$$

$$\frac{\partial \Omega_{xz}}{\partial t}+(\alpha_z+\frac{\sigma_z}{\kappa_z})\Omega_{xz}=\frac{\sigma_z}{\kappa_z^2}\frac{\partial T_{xz}}{\partial z} \tag{16b}$$

$$\frac{\partial \Omega_{zx}}{\partial t}+(\alpha_x+\frac{\sigma_x}{\kappa_x})\Omega_{zx}=\frac{\sigma_x}{\kappa_x^2}\frac{\partial T_{xz}}{\partial x} \tag{16c}$$

$$\frac{\partial \Omega_{zz}}{\partial t}+(\alpha_z+\frac{\sigma_z}{\kappa_z})\Omega_{zz}=\frac{\sigma_z}{\kappa_z^2}\frac{\partial T_{zz}}{\partial z} \tag{16d}$$

$$\frac{\partial \Psi_{xx}}{\partial t}+(\alpha_x+\frac{\sigma_x}{\kappa_x})\Psi_{xx}=\frac{\sigma_x}{\kappa_x^2}\frac{\partial V_x}{\partial z} \tag{16e}$$

$$\frac{\partial \Psi_{zz}}{\partial t}+(\alpha_z+\frac{\sigma_z}{\kappa_z})\Psi_{zz}=\frac{\sigma_z}{\kappa_z^2}\frac{\partial V_z}{\partial z} \tag{16f}$$

$$\frac{\partial \Psi_{zx}}{\partial t}+(\alpha_x+\frac{\sigma_x}{\kappa_x})\Psi_{zx}=\frac{\sigma_x}{\kappa_x^2}\frac{\partial V_z}{\partial x} \tag{16g}$$

$$\frac{\partial \Psi_{xz}}{\partial t}+(\alpha_z+\frac{\sigma_z}{\kappa_z})\Psi_{xz}=\frac{\sigma_z}{\kappa_z^2}\frac{\partial V_x}{\partial z} \tag{16h}$$

We put these eight auxiliary equations together but these equations are actually independent of each other. The auxiliary variables involved in each equation are independent, with each equation related to one spatial direction, such as the z and x directions. So, we can implement the eight equations in x and z coordinates. The right sides of the equations are partial derivatives in the original field terms. There are eighteen different spatial partial derivatives in the 3D case:

$$\frac{\partial T_{xx}}{\partial x}, \frac{\partial T_{xy}}{\partial x}, \frac{\partial T_{xz}}{\partial x}, \frac{\partial T_{xy}}{\partial y}, \frac{\partial T_{yy}}{\partial y}, \frac{\partial T_{yz}}{\partial y}, \frac{\partial T_{xz}}{\partial z}, \frac{\partial T_{yz}}{\partial z}, \text{ and } \frac{\partial T_{zz}}{\partial z}$$

and $\frac{\partial V_x}{\partial x}$, $\frac{\partial V_x}{\partial y}$, $\frac{\partial V_x}{\partial z}$, $\frac{\partial V_y}{\partial x}$, $\frac{\partial V_y}{\partial y}$, $\frac{\partial V_y}{\partial z}$, $\frac{\partial V_z}{\partial x}$, $\frac{\partial V_z}{\partial y}$ and $\frac{\partial V_z}{\partial z}$,

so eighteen auxiliary variables Ω_{ij}, ψ_{ij}, $i, j \in \{x,y,z\}$ and eighteen auxiliary equations have been introduced.

This tells us that each spatial partial derivative is related to only one auxiliary variable. All auxiliary equations have the same expression of non-homogeneous first-order partial differentials and the CFS-PML implementation is easily extended to other complex media.

Discrete numerical solution

The SPML equations or the CFS-PML auxiliary variable differential equations can both be described as:

$$\frac{\partial f}{\partial t}+\beta f=\gamma, \tag{17}$$

where $\beta \geq 0$ and its corresponding analytic solution is

$$f=-\frac{1}{\beta}e^{-\beta t}+\frac{1}{\beta}\gamma. \tag{18}$$

Equation (18) also can written in discrete form as

$$\begin{aligned} f[(n+1)\Delta t]&=-\frac{1}{\beta}e^{-\beta\Delta t}e^{-\beta n\Delta t}+\frac{1}{\beta}\gamma, \\ f[n\Delta t]&=-\frac{1}{\beta}e^{-\beta n\Delta t}+\frac{1}{\beta}\gamma, \end{aligned} \tag{19}$$

Thus we have

$$f[(n+1)\Delta t]=e^{-\beta\Delta t}f[n\Delta t]+\frac{1}{\beta}(1-e^{-\beta\Delta t})\gamma \tag{20}$$

Taking equation (16-a) as an example, we can easily write its discrete numerical expression to solve for auxiliary variables:

$$\begin{aligned} \Omega_{xx}^{n+1}=&\exp[-(\alpha_x+\frac{\sigma_x}{\kappa_x})\Delta t]\Omega_{xx}^n \\ &+\frac{\sigma_x}{\kappa_x(\kappa_x\alpha_x+\sigma_x)}\left\{1-\exp[-(\alpha_x+\frac{\sigma_x}{\kappa_x})\Delta t]\right\}\frac{\partial T_{xx}^{n+1/2}}{\partial x} \end{aligned} \tag{21}$$

This expression and the discrete numerical expression in Komatitsch and Martin (2007) is similar in form. The difference is that Komatitsch and Martin (2007) used a convolution operator with a recursion integral and the corresponding formula derivation is complex, whereas we combined convolution with the analytical solution of non-homogeneous first-order differential equations and the differential equations of the auxiliary variables are

derived to get the numerical solution of the equation.

Other auxiliary variables corresponding to the differential equations have the same form of expression and their numerical solution follows the same formula, as well as their discrete solutions. Taking the third equation in equation (1) as an example, we can derive the discrete numerical solution of T_{xx} and its auxiliary variables ψ_{xx} and ψ_{zz} as

$$\begin{cases} T_{xx}^{n+1} = T_{xx}^{n} + \Delta t(\lambda+2\mu)\dfrac{\partial V_x^{n+1/2}}{\partial x}, (T_{xx} \text{ updates in x direction}) \\ T_{xx}^{n+1} = T_{xx}^{n+1} - \Delta t(\lambda+2\mu)(c_x \dfrac{\partial V_x^{n+1/2}}{\partial x} + \Psi_{xx}^{n}), (T_{xx} \text{ attenuates in x direction}) \\ \Psi_{xx}^{n+1} = b_x \Psi_{xx}^{n} + a_x \dfrac{\partial V_{xx}^{n+1/2}}{\partial x}, (\Psi_{xx} \text{ updates in x direction}) \\ T_{xx}^{n+1} = T_{xx}^{n+1} + \Delta t\lambda \dfrac{\partial V_z^{n+1/2}}{\partial z}, (T_{xx} \text{ updates in z direction}) \\ T_{xx}^{n+1} = T_{xx}^{n+1} - \Delta t\lambda(c_z \dfrac{\partial V_z^{n+1/2}}{\partial z} + \Psi_{zz}^{n}), (T_{xx} \text{ attenuates in z direction}) \\ \Psi_{zz}^{n+1} = b_x \Psi_{zz}^{n} + a_z \dfrac{\partial V_{zz}^{n+1/2}}{\partial z}, (\Psi_{zz} \text{ updates in z direction}), \end{cases} \quad (22)$$

where

$$c_p = (1-\frac{1}{\kappa_p}),\ b_p = \exp[-(\alpha_p + \frac{\sigma_p}{\kappa_p})\Delta t],$$

$$a_p = \frac{\sigma_p}{\kappa_p(\kappa_p\alpha_p + \sigma_p)}(1-b_p),$$

and $(p=x,z)$. The difference operator $\frac{\partial}{\partial x}$, $\frac{\partial}{\partial z}$ can be computed using the implicit high-order finite difference, implicit difference, and pseudo-spectral methods. From equation (21), it can be seen that our CFS-PML numerical implementation scheme is much simpler.

The CFS parameters

In theory, there will be no reflection and attenuation when waves propagate in the PML medium with the same elastic parameters (ρ,λ,μ) and the different attenuation parameters (κ,σ,α). The conventional wave equation is a special case of the PML wave equation when $\kappa=1,\sigma=0,\alpha=0$. However, the finite-difference discrete numerical method can cause numerical reflections at different PML interfaces. To reduce the unexpected reflections, we can try to make these PML attenuation parameters change smoothly. Collino and Tsogka (2001) use the polynomial function to set the CFS parameter σ:

$$\sigma_p^{\max} = -\frac{3v}{2d}\ln(R), \sigma_p(l) = \sigma_p^{\max}\left(\frac{l}{d}\right)^m, (p=x,y,z), \quad (23)$$

where $l(0\le l\le d)$ is the distance from the PML outside boundary to the PML inside boundary, d is the thickness of the PML area, m is the order of the polynomial (equal to 1 or 3), R is the theoretical reflection coefficient (in the range of 0.001 - 0.00001, and v is the P-wave velocity in the PML area. The other two attenuation parameters are set as

$$\kappa_p = 1 + (\kappa_p^{\max} - 1)\left(\frac{l}{d}\right)^m, (p=x,y,z), \quad (24)$$

$$\alpha_p = \alpha_p^{\max}\left(\frac{l}{d}\right)^m, (p=x,y,z). \quad (25)$$

The two equations (24) and (25) are common equations, which can also be described using other continuous-change functions.

PML algorithm analysis and model test

Several conventional PML ABC algorithms are compared in Table 1 with the improved PML ABC algorithm in this paper and the SPML ABC implementations are generally divided into global and local schemes. In the global SPML scheme, all areas are regarded as perfectly matched layers, simple to realize but the number of split variables is three or four times greater than original variables. So the method needs a large memory for computing the split variables. In the two dimension elastic wave equation case, there are five original variables but the number of variables increases to 15 using the global SPML scheme. In the 3-D case, there are nine original variables, which increase to 33 using the global SPML scheme. The increased auxiliary variables will be used for calculations over the entire area. In the local SPML scheme, the PML wave equation is only used in the boundary area. However, in this scheme, the faces, edges, and corners of the calculated area boundary must be considered separately, For example, in the 3-D case, there are twenty-four auxiliary variables for each of the total twenty-six areas: six faces, twelve edges, and eight corners for a total of 624 variables to be computed. The programming realization becomes very complex.

The NPML implementation directly calculates the convolution operation, also a very large number of calculations. The number of auxiliary variables in the 2D and 3D cases are eight and eighteen, respectively. These auxiliary variables are only used in the PML boundary region, so calculations and updating is not necessary for the complex face, edge, and corner regions. For the 3-D case, compared to the traditional PML boundary conditions, the realization of the NPML absorbing boundary conditions can achieve a more flexible design of the attenuation parameters, the calculation equations are simple, programming is easy, and memory use is small. Especially, for ABCs for 3-D wave equations, our implementation scheme has large advantages.

Table 1 Comparing several types of PML schemes

Type		2D				3D			
		local SPML	global SPML	conventional NPML	improved NPML	local SPML	full SPML	conventional NPML	improved NPML
Original variables		5	10	5	5	9	24	9	9
Auxiliary variables		10	0	16	8	24	0	36	18
Absorbing boundary	faces	0	0	0	0	6	0	6	6
	edges	4	0	4	4	12	0	0	0
	corners	4	0	0	0	8	0	0	0
Programming		complex	simple	complex	simple	complex	simple	complex	simple
CFS		No	No	Yes	Yes	No	No	Yes	Yes

In order to test our improved NPML ABC absorption and attenuation properties, we design a 2D numerical model. This model has two layers, with a model mesh size of 400 × 80 with a spatial interval in both horizontal and vertical directions of 7.5 m. The total number of samples is 1900 with a time interval of 0.6 ms. In the first layer, the P-wave velocity is 2500 m/s, the S-wave velocity is 1440 m/s, the density is 2000 kg/m^3, and the layer thickness is 450 m. In the second layer, the P-wave velocity is 3600 m/s, the S-wave velocity is 2080 m/s, the density is 2300 kg/m^3, and the layer thickness is 150 m. We select a 25 Hz Ricker wavelet as the source, located at 750 m by 82.5 m. Each of the four boundaries has ten PML layers with layer thicknesses of 75 m and there is only one mesh interval from the source location to the PML inside boundary. To realize the spatial derivatives, we use high-order finite differences with a half finite difference operator using ten nodes, i.e., the spatial first-order partial derivative calculation involves the values of twenty grid nodes around it and the resulting precision is close to the pseudo-spectral method.

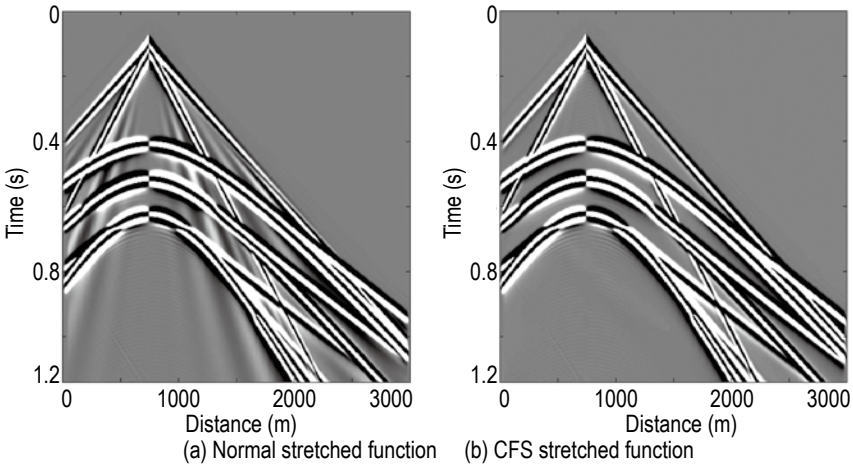

Fig. 1 Horizontal particle velocity records with NPML ABC.

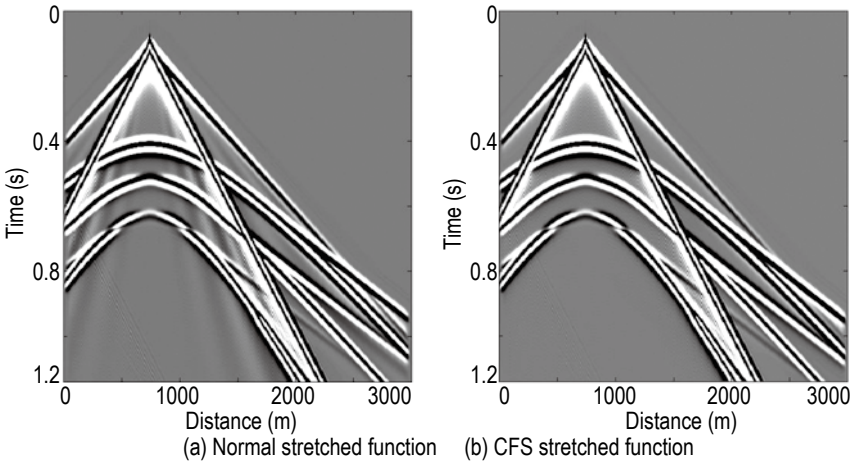

Fig. 2 Vertical particle velocity records with NPML ABC.

The seismic records were simulated using both the CFS stretched function and the normal stretched function for comparison. For the normal stretched function, the parameters are set as: κ=2, σ =1100, and α = 150. For the CFS stretched function, the parameters are set as k = 1, σ =1500, and α = 0. The simulated horizontal particle velocity seismic records are shown in Figure 1 and the vertical particle velocity records are shown in Figure 2. From these two figures we can see the direct P-wave, the direct S wave, the P-wave reflection, the S-wave reflection, converted-waves, and refracted waves but boundary reflections are not observed. The source depth of these records is same. From the left panels of Figures 1 and 2 we see that some low-frequency interference associated with the direct arrivals which is not observed in the right panels.

Figures 3 and 4 show the 150th trace of the horizontal and vertical component records from Figures 1 and 2. The solid line is the CFS stretched function and the dotted line is the normal stretched function. From the left panels of the Figures 3 and 4, it appears that the records obtained using the two methods agree well. However, when the amplitude of the trace was enlarged 1000 times (right panels), the amplified traces don't agree with each other, as shown by the arrows. Though the interference effects are small for the records, we can still eliminate these small interferences by designing reasonable CFS parameters.

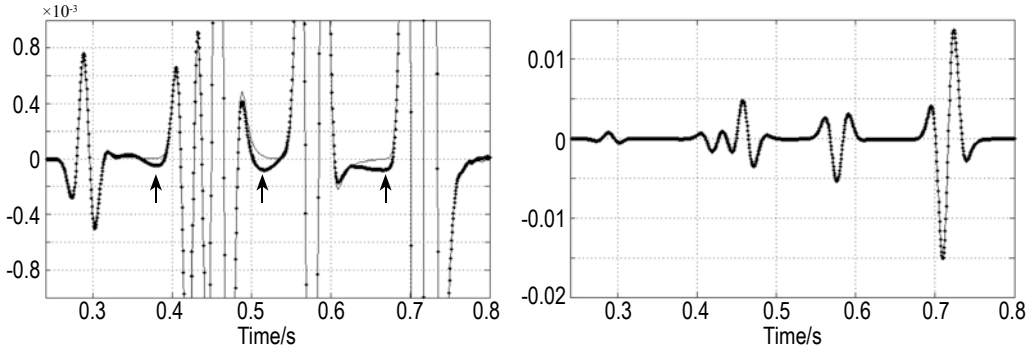

Fig. 3 Comparison of the 150th trace from Figures 1a and 1b. The solid line is the CFS stretched function and the dotted line is the normal stretched function.

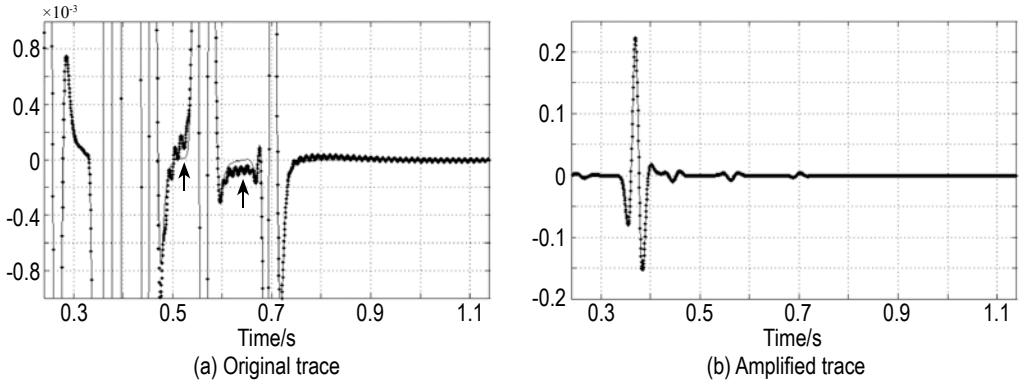

Fig. 4 Comparing the 150th trace from Figures 2a and 2b. The solid line is the CFS stretched function and the dotted line is the normal stretched function.

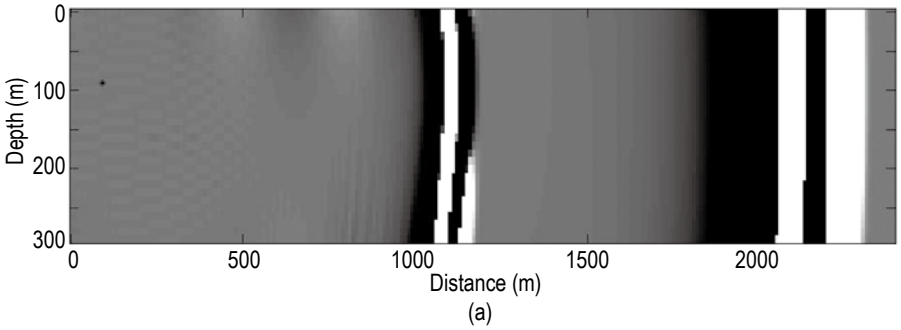

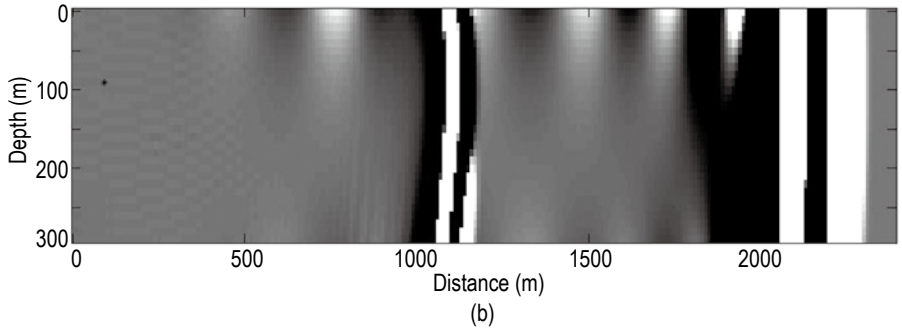

Fig. 5 Comparison of the wave-fields. The upper panel uses the CFS stretched function (a) and the lower panel uses the normal stretched function (b).

Figure 5 shows snapshots of wavefields using the CFS PML (upper panel) and the normal PML (lower panel). In order to clearly observe the reflection energy, the wavefields are amplified by 600 times. Because the source is very near the PML inner boundary, the wave propagates almost horizontally, i.e., the incident angle is close to 90° at the PML area away from the seismic source. From comparing the wavefield snapshots in the Figure 5, we see that the greater the incident angle, the poorer the ABCs absorbing property. However, the improved CFS-PML ABCs still has good absorption even when the incidence angle is larger than 90 degrees.

Conclusions

In this paper, we presented a new implementation of the CFS-PML absorbing boundary conditions, which is an extension of the traditional NPML ABC implementation. Based on the CFS stretched function, we can decompose the elastic wave equation for PML media into normal and attenuated terms by introducing intermediate auxiliary variables. The normal term calculation is over the entire section, including the PML boundary region, but the attenuated term calculation is only performed in the PML region. As a result, the calculating equations of the attenuation term are simple non-homogeneous differential equations, not integral equations, and it is easy to deduce the corresponding numerical formula. This method does not involve the convolution operation. The CFS stretched function does not increase the numerical realization difficulty and the attenuation parameter design is more flexible.

The test results show that the proposed NPML absorbing boundary condition has a better absorption effect. If the new method can be applied to the other wave equation types, we only need to add an attenuation term for the spatial derivative term and the resulting equation is a simple differential equation. Our method is based on the first-order partial differential wave equation, applying it to the second-order partial differential wave equation needs further study.

Acknowledgements

The authors thank the anonymous reviewers for their comments to improve the original manuscript.

References

Appelö, D., and Kreiss, G., 2006, A new absorbing layer for elastic waves: Journal of Computational Physics, **215**(2), 642 – 660.

Basu, U., and Chopra, A. K., 2004, Perfectly matched layers for transient elastodynamics of unbounded domains: International Journal for Numerical Methods in Engineering, **59**(8), 1039 – 1074.

Bérenger, J. P., 1994, A perfectly matched layer for absorption of electromagnetic waves: Journal of Computational Physics, **114**(2), 185 – 200.

Chen, Y. H., Chew, W. C., and Oristaglio, M. L., 1997, Application of perfectly matched layers to the transient modeling of subsurface EM problems: Geophysics, **62**(6), 1730 – 1736.

Chew, W. C., and Weedon, W. H., 1994, A 3-D perfectly matched medium from modified Maxwell's equations with stretched coordinates: Microwave and Optical Technology Letters, **7**(13), 599 – 604

Chew, W. C., and Liu, Q. H., 1996, Perfectly matched layers for elastodynamics: A new absorbing boundary condition: Journal of Computational Acoustics, **4**(4), 341 – 359.

Cohen, G., and Fauqueux, S., 2005, Mixed spectral finite elements for the linear elasticity system in unbounded domains: SIAM Journal on Scientific Computing, **26**(3), 864 – 884.

Collino, F., and Tsogka C., 2001, Application of the PML absorbing layer model to the linear elastodynamic problem in anisotropic heterogeneous media: Geophysics, **66**(1), 294 – 307.

Drossaert, F. H. and Giannopoulos, A., 2007, A nonsplit complex frequency-shifted PML based on recursive integration for FDTD modeling of elastic waves: Geophysics, **72**(2), T9 – T17.

Festa, G., and Nielsen S., 2003, PML absorbing boundaries: Bulletin of the Seismological Society of America, **93**(2), 891 – 903.

Festa, G., and Vilotte, J. P., 2005, The Newmark scheme as velocity-stress time-staggering: An efficient PML implementation for spectral-element simulations of elastodynamics: Geophysical Journal International, **161**(3), 789 – 812.

Hastings, F. D., Schneider, J. B., and Broschat, S. L., 1996, Application of the perfectly matched layer (PML) absorbing boundary condition to elastic wave propagation: Journal of the Acoustical Society of America, **100**(5), 3061 – 3069.

Higdon, R. L., 1991, Absorbing boundary condition for elastic waves: Geophysics, **56**(2), 231 – 241.

Komatitsch , D., and Martin, R., 2007, An unsplit convolutional perfectly matched layer improved at grazing incidence for the seismic wave equation: Geophysics, **72**(5),SM155 – SM167

Komatitsch, D., and Tromp J., 1999, Introduction to the spectral-element method for 3-D seismic wave propagation: Geophysical Journal International, **139**(3), 806 – 822.

Kuzuoglu, M., and Mittra, R., 1996, Frequency dependence of the constitutive parameters of causal perfectly matched anisotropic absorbers: IEEE Microwave and Guided Wave Letters, **6**(2), 447 – 449.

Liao, Z. P., Wong, H. L., and Yuan, Y. F., 1984, A transmitting boundary for transient wave analysis: Scientia Sinica, **27**(6), 1063 – 1076.

Ma, S., and Liu, P., 2006, Modeling of the perfectly matched layer absorbing boundaries and intrinsic attenuation in explicit finite-element methods: Bulletin of the Seismological Society of America, **96**(5), 1779 – 1794.

Marfurt, K. J., 1984, Accuracy of finite-difference and finite-element modeling of the scalar and elastic wave equation: Geophysics, **49**(5), 533 – 549.

Rappapport, C. M., 1995, Perfectly matched absorbing boundary conditions based on anisotropic lossy mapping of space: IEEE Microwave Guided Wave Lett., **5**(3), 90 – 92.

Shin, C., 1995, Sponge boundary condition for frequency-domain modeling: Geophysics, **60**(6), 1870 – 1874.

Song R. L., Ma J., and Wang K. X., 2005, The application of non-splitting perfectly matched layer in numerical modeling of wave propagation in poroelastic media: Applied geophysics, **2**(4), 216 – 222.

Teixeira, F. L., and Chew, W. C., 1999, On causality and dynamic stability of perfectly matched layers for FDTD simulations: IEEE Transactions on Microwave Theory and Techniques, **47**(6), 775 – 785.

Tsili, W. and Tang, X. M., 2003, Finite-difference modeling of elastic wave propagation: A nonsplitting perfectly matched layer approach: Geophysics, **68**(5), 1749 – 1755.

Wang, T., and Oristaglio, M. L., 2000, 3-D simulation of GPR surveys over pipes in dispersive soils: Geophysics, **65**(5), 1560 – 1568.

Qin Zhen received his master from Jianghan Petroleum University in 2004 and received his PhD from the China University of Geosciences in Wuhan in 2008. Currently, he is a post-doctor at the Research Institute of Petroleum Exploration & Development. His research work mainly focus on seismic pre-stack denoising, geophysical forward modeling, and geophysical inverse problems.